**Opposite role of different carbon fiber reinforcements on the non-isothermal crystallization behavior of poly(etheretherketone)**

**Opposite role of different carbon fiber reinforcements on the non-isothermal crystallization behavior of poly(etheretherketone)**

Marco Regis[1,2], Marco Zanetti[1], Michele Pressacco[2], Pierangiola Bracco[1,*].

[1] Department of Chemistry and NIS (Nanostructured Interfaces and Surfaces) Centre, University of Turin, Turin, Italy

[2] R&D Department, Limacorporate SpA, Villanova di S. Daniele (UD), Italy

[*]Corresponding author:

Pierangiola Bracco
Department of Chemistry and NIS Center,
University of Turin,
Via Pietro Giuria, 7
10125 Torino, ITALY
Phone: +39 011 6707547
Fax: +39 011 6707855
e-mail: pierangiola.bracco@unito.it

**(*Running title*: Non-isothermal crystallization behavior of CFR-PEEK)**

**Highlights:**

- A non isothermal crystallization study for PEEK and two CFR PEEK is proposed
- Fibers influence the polymer crystallization by either favoring or hindering it
- Fibers and processing conditions must be considered for optimal polymer morphology

**Graphical abstract.**

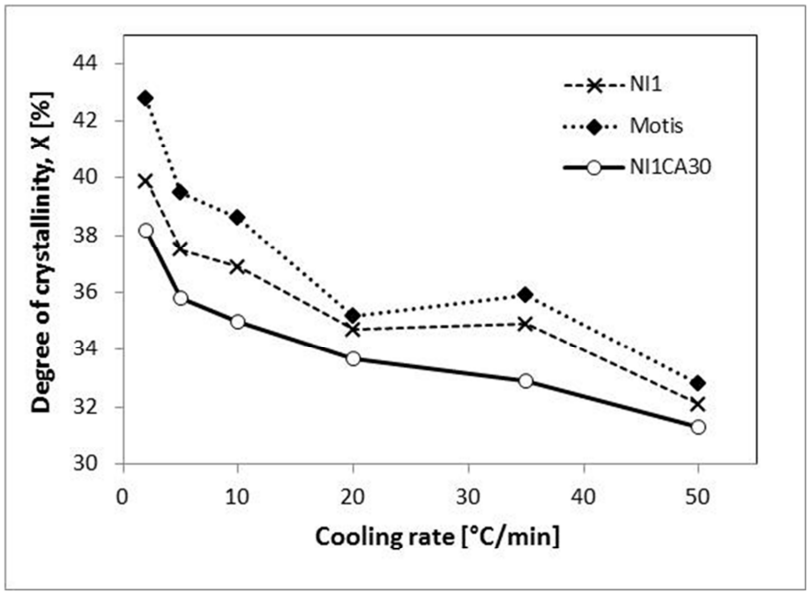

**Abstract**

A non-isothermal crystallization study on two different 30%w carbon fiber (PAN and pitch-based) reinforced PEEK was performed by differential scanning calorimetry (DSC), aiming to provide more information on PEEK crystallization behavior in the presence of reinforcements. Melt crystallization was performed by cooling down the CFR-PEEK samples from the molten state with different cooling rates (from 2 to 50°C/min). Samples were subsequently heated up again at 400°C at 20°C/min to evaluate any potential differentiation in the created crystal structures. The same experiments were run also for unfilled PEEK, taken as reference. Crystallization kinetics (with Avrami and Avrami-Ozawa approaches), and activation energies (according to Friedman method) were evaluated. The results showed that the cooling rate influences crystal growth and morphology but also, more importantly, that fiber type affects the crystallization mechanisms, either favoring or hindering polymer crystallization, depending on the fiber characteristics, geometry and density. Overall, these observations suggest that accurate fiber selection and processing conditions set up have to be chosen to ensure an optimal polymer morphology.

## 1. Introduction

In the last decades, poly(etheretherketone) (PEEK) has been shown to be one of the most promising structural polymers for a wide range of industrial sectors, such as aerospace, biomedical, and high temperature applications, due to its high transition temperature and strong chemical resistance to various agents [1,2]. More recently, also PEEK composites have been looked at as promising materials, thanks to their enhanced mechanical properties and strength to weight ratio [3].

As for every semi-crystalline polymer, PEEK properties largely depend upon molecular weight and crystallinity. Due to its high melting temperature, the processing conditions are often highly demanding, implying high temperatures (up to 400°C) and sensitive cooling steps, which affect the polymer morphology. For this reason, a considerable amount of research has been carried out to determine the influence of the thermal history on PEEK crystallinity and crystallization behavior, often with controversial results [4–7]. Univocally, it was found that PEEK exhibits a double melting peak, despite different interpretations have been given for such behavior [8–10]. Nowadays, the most acknowledged theory is based on a combination of the simultaneous partial melting and recrystallization of the polymer crystal domains [7,11]. Several studies, based on different techniques (i.e. DSC, WAXS/SAXS, FT-IR, etc.) supported this indication [6,12,13].

When studying PEEK crystallization behavior, both isothermal and non-isothermal approaches have been used [5,11,14,15]. Kinetic aspects of the crystallization process were usually described by the

Avrami theory or alternative methods [14,16,17], but studies performed so far are often discordant and most models were proven to be inadequate to some extent, especially when considering the addition of reinforcements [3,7,18,19], to the point that no clear indication on the effect of the reinforcement on the crystallization behavior of the polymer can be obtained.

Therefore, providing more data on PEEK composites crystallization behavior, as a function of the reinforcement typology and characteristics, is still needed to understand the crystallization mechanism of the final composite material.

The present work investigates PEEK crystallization in the presence of two different carbon fiber reinforcements (CFR). The use of a non-isothermal approach has been preferred, since PEEK and PEEK composites processing (i.e. extrusion or compression molding) is usually performed under dynamic non-isothermal conditions. It is therefore of interest to provide information on the effect of thermal history on the crystalline structure of the considered materials, in the presence of fibers with different characteristics. The results obtained on the composites were compared with those of non-reinforced PEEK, in order to assess any deviation from the crystallization of the neat polymer.

## 2. Materials and methods

The materials of choice for the study were an unfilled biomedical grade PEEK (NI1) and two formulations of biomedical grade 30% wt. carbon fiber reinforced (CFR) PEEK, PAN and pitch based, named NI1CA30 and Motis, respectively (Invibio, UK). Only 30% wt. formulations are available for biomedical applications, therefore different reinforcement percentages were not considered. The carbon fibers have different mechanical properties, dimensions, and densities: Young's modulus and fiber diameter are 540 GPa and 6±2 μm for PAN carbon fibers, and 280 GPa and 10±2μm for pitch carbon fibers, respectively, while density is 1.76g/cm$^3$ and 2 g/cm$^3$ for PAN and pitch carbon fibers, respectively [20].

Melt crystallization DSC studies were carried out to assess the crystallization behavior of the selected materials. As mentioned in the introduction, non-isothermal melt crystallization was chosen in spite of a more conventional isothermal approach to better simulate the processing conditions of PEEK and CFR-PEEK. Cold crystallization has not been considered since the transformation process implies a cooling step from the molten state, rather than heating steps from the glassy state.

The non-isothermal melt crystallization studies were carried out in a TA Q20 DSC (TA inc, USA). 6.5 to 8.5 mg samples were encapsulated in hermetic pans. The first DSC step was a preliminary heating up stage at 400°C for 15 minutes, to erase previous thermal history and ensure a nuclei-free melt. This procedure is generally applied in non-isothermal studies, since it allows to erase the

previous thermal effects on the polymer, i.e. crystallization during processing conditions, and ensures that crystallization behavior observed during the study is not significantly influenced by the sample preparation procedure [3,21]. After the heating step, samples were cooled down to 30°C at different cooling rates (2, 5, 10, 20 and 50°C/min). Although thermal lag is known to affect the accuracy of the DSC results [22], a number of studies have demonstrated that it has a moderate effect within the range of cooling rates and sample masses investigated here [9,22]. The selected cooling rates are considered to be representative of a standard injection molding process. Typically, injection molded material is kept at a temperature above the $T_m$ (usually 400°C or slightly less) as it flows inside the mold, which is kept at a lower temperature, e.g. 250°C. Polymer flow and holding time usually takes 2-3 minutes, depending upon the complexity of the part to be realized, then the molds are opened and the molded polymer shape is naturally cooled in air, where it reaches RT within 5 minutes. With these processing steps, it is believed that the overall cooling rate of the material should range from around 30-50°C/min to 100-150°C/min, which partly overlaps the selected cooling rates. All tests were run in triplicate. The DSC apparatus was calibrated with indium and zinc for each of the cooling rates used in this study.

After the crystallization study, the resulting samples were subjected to an additional heating run, up to 400°C at 20°C/min. Samples were then held at 400°C for 5 minutes and cooled down to 30°C at 20°C/min .

% Crystallinity was calculated as

$$X\% = \frac{\Delta H_f}{\Delta H_f^0 \cdot \nu_m} \cdot 100 \quad (1)$$

where $\Delta H_f^0$=130 J/g is the theoretical heat of fusion of pure crystalline PEEK [4] and $\nu_m$ is the polymer content.

## 3. Results and discussion.

### *3.1 Non-isothermal crystallization behavior*

The crystallization exotherms of pure, unreinforced PEEK and of both CFR PEEK formulations at different cooling rates are presented in Figure 1.

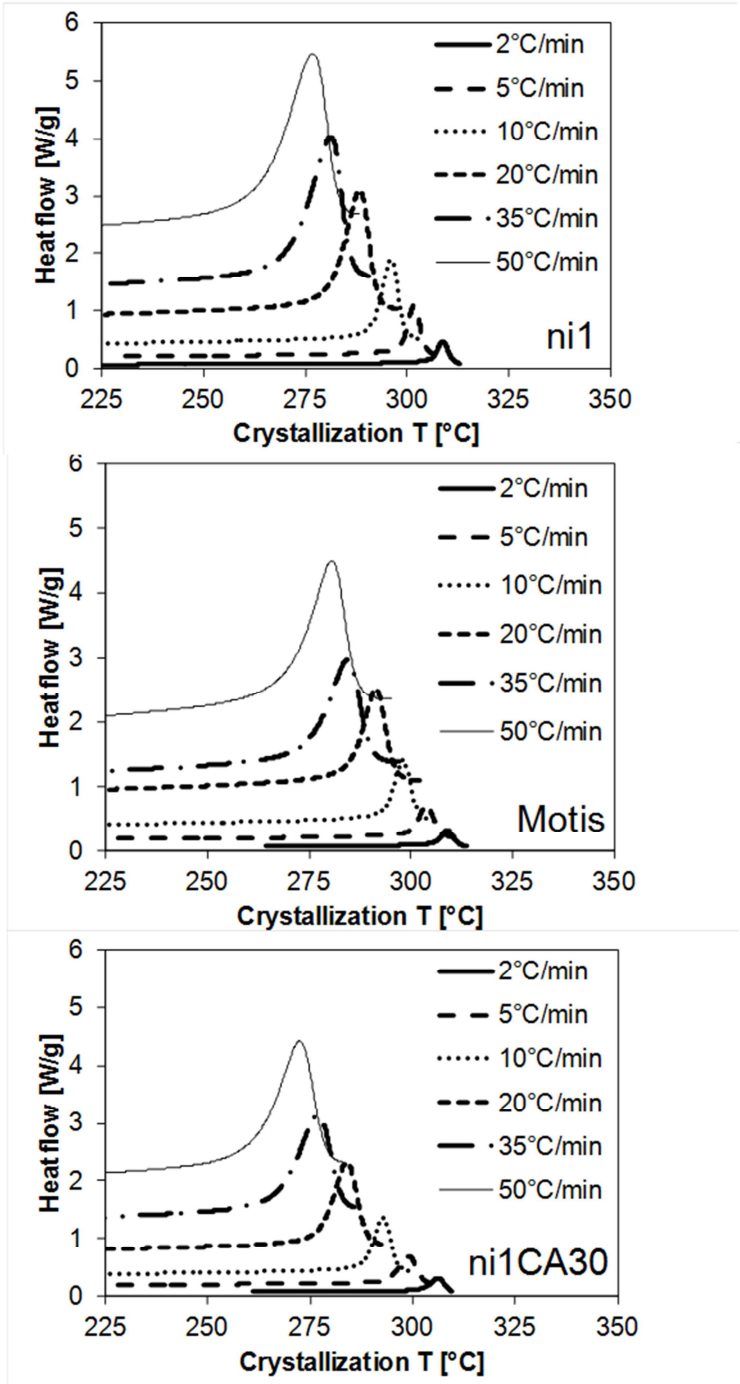


Figure 1. crystallization exotherms at different cooling rates for each material tested.

The crystallization enthalpies (Table 1), calculated from the area under the DSC curve and corrected for the actual weight ratio of the polymer (70%) in the two CFR formulations, decrease as the cooling rate increases, as can be expected due to a shorter time allowed for crystallization, which will result in a lower total crystallinity. Only slight differences were observed among the three formulations: at low cooling rates (≤10°C min), the crystallization enthalpy of NI1CA30 is constantly lower than that of NI1 and Motis.

| Cooling rate [°C/min] | $T_c$[°C] | | | Corrected $\Delta H_c$ [J/g] | | |
|---|---|---|---|---|---|---|
| | NI1 | NI1CA30 | Motis | NI1 | NI1CA30 | Motis |
| **2** | 309 | 306 | 309 | 56.1±0.3 | 51.3±0.3 | 53.6±0.4 |
| **5** | 302 | 299 | 304 | 54.6±2.2 | 52.1±0.2 | 57.1±0.4 |
| **10** | 296 | 293 | 298 | 53.8±0.8 | 51.7±0.2 | 52.5±0.1 |
| **20** | 288 | 284 | 291 | 51.5±0.5 | 54.1±0.3 | 48.9±0.2 |
| **35** | 281 | 277 | 284 | 46.0±0.2 | 42.9±0.5 | 42.5±0.1 |
| **50** | 276 | 272 | 281 | 43.7±0.8 | 43.6±0.1 | 45.4±0.3 |

Table 1. $T_c$ and corrected ΔH for NI1, Motis, and NI1CA30 at each crystallization rate considered.

The peak crystallization temperature ($T_c$) of the unfilled material decreases as the cooling rate increases (Table 1 and Figure 2), since crystallization time at higher cooling rates is lower.
The same behavior has been observed also for the two CFR formulations, although slightly higher and lower $T_c$ have been found for Motis and N1CA30 CFR-PEEK respectively, when compared to neat PEEK.

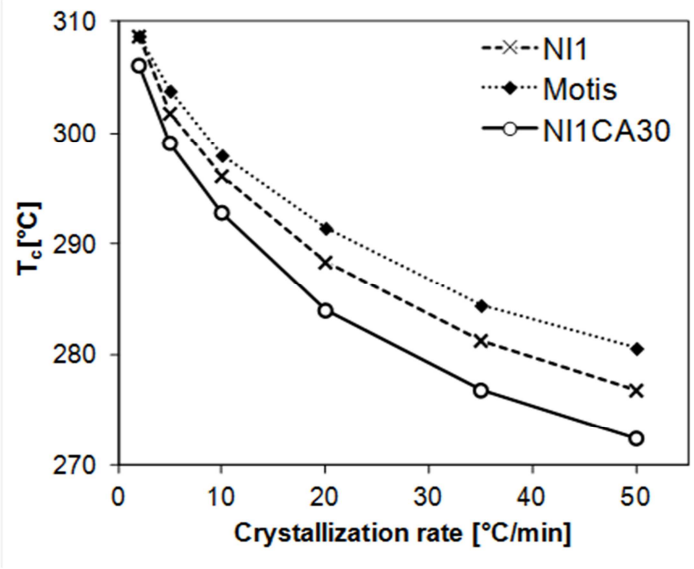


Figure 2. Crystallization temperature ($T_c$) as a function of cooling rate for each PEEK formulation tested.

According to what reported in previous literature studies [3,18,19], there are two major mechanisms affecting the crystallization of PEEK composites: heterogeneous nucleation and mobility of chain segments. When comparing the behavior of a CFR PEEK to that of neat PEEK, if heterogeneous nucleation is dominating, crystallization will occur at lower supercooling (i.e. $T_c$ will be shifted to higher values); conversely, if the presence of the filler results in predominating hindrance of mobility of chain segments, $T_c$ will be shifted to lower values. Additionally, the filler was proposed to have an influence, under cooling rates slower than the critical cooling rate to obtain non-

crystalline material, on the amount of nuclei available for cold crystallization, either preventing or favoring the crystallization phenomena [23].

We should therefore hypothesize that the two CF reinforces play an opposite role on PEEK crystallization: pitch fibers favoring heterogeneous nucleation, while PAN fibers hindering the molecular mobility and resulting in a lower overall crystallization. It must be taken into account that, given the different fibers density and dimensions, a higher amount of fibers per volume is required for PAN fibers, compared to pitch fibers, to achieve the same weight percentage. Hence, a higher fiber density will result in restricted spaces between fibers, reducing the crystallization ability of the PAN composite.

### *3.2 Crystallization kinetic*

The relative crystallinity $X(t)$ during the crystallization step at different cooling rates was calculated as the cumulative percentage of the correspondent DSC thermogram peak and plotted as a function of crystallization time t (Figure 3), expressed as:

$$t = \frac{T_0 - T}{a} \tag{2}$$

where $a$ represents the cooling rate and $T_0$ the onset temperature of crystallization.

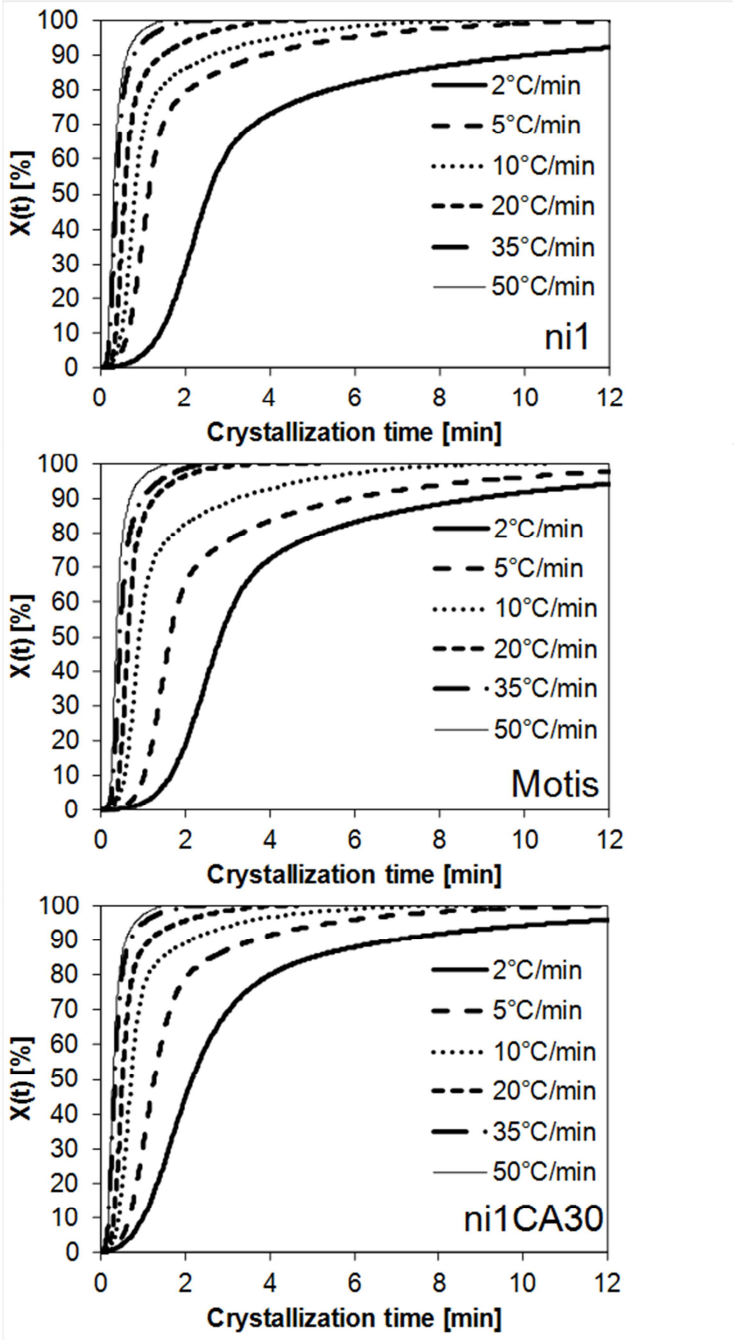


Figure 3. Development of relative crystallinity with time at different cooling ramps, for NI1, Motis and NI1CA30.

Trend in crystallization is sigmoidal, as reported elsewhere [7,11,24]. The cooling rate affects the crystallization rate, as for slower cooling ramps the amount of crystallization at a given t is lower, resulting in incomplete crystallization, within the time interval represented in the plots, at the lower cooling rates. The latter portion of the curves, where the crystallization rate is significantly slowed down, could be influenced by the spherulites impingement in the later stage of crystallization. Previous literature studies [14,17,24] attributed this behavior to the existence of two crystallization

processes: a fast “primary” process, during the initial stage and a slower “secondary” process during the later stage of crystallization.

The opposite effect of the two reinforcements in respect to the unfilled material is confirmed by observing the overall crystallization times (Figure 4a). Crystallization time is longer for the pitch CFR PEEK formulation (Motis), while it decreases, if compared to that of neat PEEK, for the PAN CFR PEEK material (N1CA30). Moreover, the onset temperature ($T_0$) of the exothermic crystallization peak of pitch CFR PEEK is always higher than that of the unfilled material (Figure 4b), while that of PAN based CFR PEEK is constantly lower. This indicates that in case of pitch CF, crystallization is favored by the presence of the fibers, while, in the case of PAN CF, the opposite effect is achieved, this meaning that the folding of chains into ordered structures is less favored. Accordingly, the total crystallization time is longer for the pitch CFR material if compared to unfilled and PAN CFR, respectively. At higher cooling rates, when the slow secondary crystallization process is less significant, this phenomenon is less pronounced.

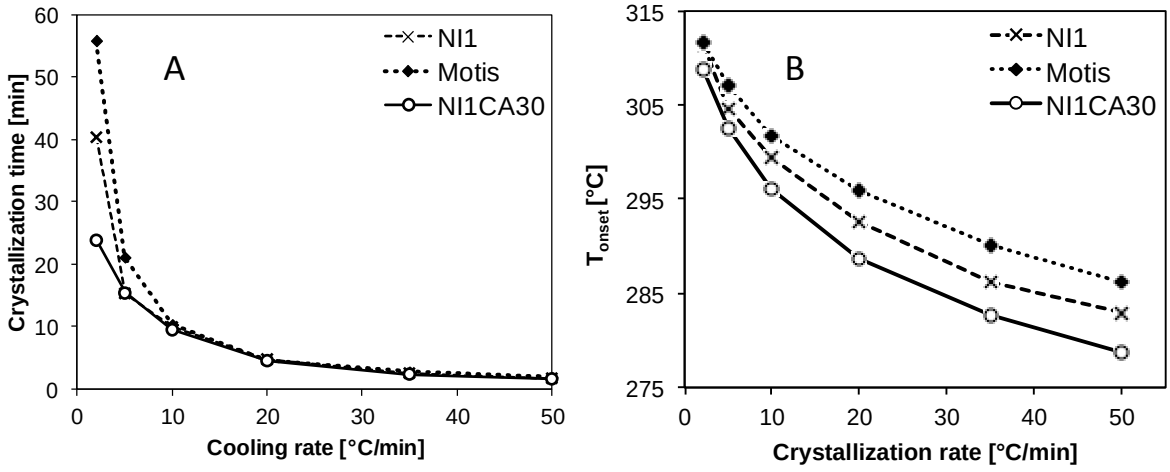


Figure 4: a) Crystallization time as a function of cooling rate and b) Onset crystallization temperature ($T_0$) as a function of cooling rate, for each PEEK formulation tested

### *3.3 Crystallization activation energy*

Crystallization activation energies have been calculated by using the Friedman iso-conventional method instead of the more traditional Kissinger approach, since it is considered to be more consistent with a non-isothermal crystallization study [25]. With this approach, the kinetic equation for a given process may be written as

$$\frac{d\alpha}{dt} = K(T)f(\alpha) \tag{3}$$

where K(T) is the Arrhenius constant, α is the conversion degree, and f(α) is the function describing the reaction mechanism. When analyzing DSC data, the conversion degree may be defined as

$$\alpha = \frac{H}{Q} \tag{4}$$

where H is the amount of heat involved in a reaction at a conversion degree α, and Q is the total amount of heat involved in the overall reaction. The kinetic equation, in the logarithmic form, therefore becomes:

$$\ln\left(\frac{d\alpha}{dt}\right) = \ln(A_\alpha f(\alpha)) - \frac{E_\alpha}{RT_\alpha} \tag{5}$$

where $A_\alpha$, $E_\alpha$, and $T_\alpha$ are the pre-exponential factor, the effective activation energy and temperature at a given conversion degree α, respectively.

Figure 5 shows the ln(dα/dt) versus 1/T plot for all the PEEK formulations, for conversion degrees of 0.1, 0.3, 0.5, 0.7 and 0.9. The activation energies for the crystallization process at a given conversion degree can be derived from the slope of the lines and are reported in Table 2.

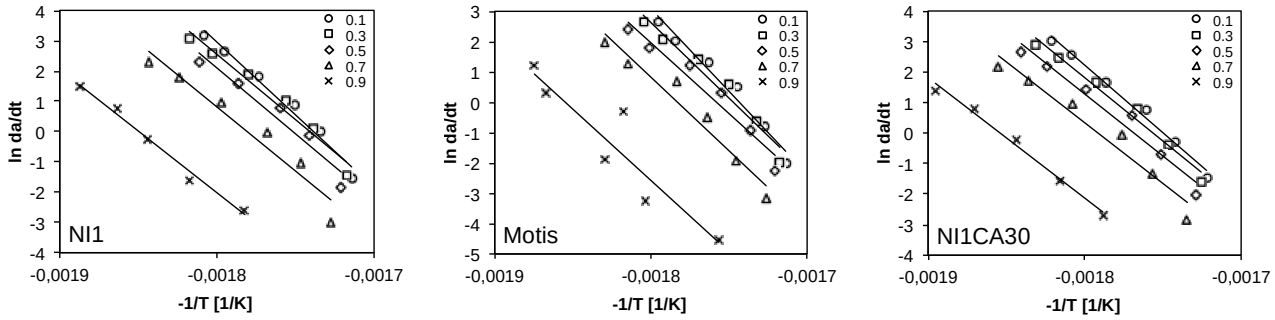


Figure 5. Friedman curves for unfilled PEEK, CFR PEEK Motis and CFR PEEK optima; conversion degrees ranging from 0.1 to 0.9.

| **Conversion degree α** | **NI1 $E_\alpha$ [kJ]** | **NI1CA30 $E_\alpha$ [kJ]** | **Motis $E_\alpha$ [kJ]** |
|---|---|---|---|
| 0.1 | -399 | -368 | -452 |
| 0.3 | -359 | -346 | -413 |
| 0.5 | -360 | -338 | -388 |
| 0.7 | -351 | -330 | -403 |
| 0.9 | -339 | -327 | -391 |

Table 2. crystallization activation energies as a function of the conversion degree α

The activation energies increased from -399 to -339 kJ, from -368 to -327kJ, and from -452 to -391kJ, with increasing the conversion degree, for unfilled PEEK, PAN CFR PEEK and pitch CFR PEEK respectively.

This indicates that the crystallization process is easier for the early stages of crystallization, while it becomes more difficult once the majority of crystallinity has been achieved [26].

It can be noted that, for each degree of conversion, once again pitch CF addition results in a lowering of the activation energy, if compared to neat PEEK, while the addition of a PAN CF reinforcement results in the opposite effect, enhancing the energy barrier to achieve the formation of crystals. This confirms the previous interpretation of the crystallization behavior and indicates that the addition of the same weight percentage of fibers of different nature (geometry, origin, density, etc) can influence the crystallization behavior of PEEK by either improving or impeding crystal growth.

### *3.4 Kinetic analysis by Avrami equation*

The crystallization kinetic have been further analyzed with the Avrami approach [27–29]. Under isothermal crystallization conditions, the Avrami equation describes the crystal growth by means of n and $Z_t$ coefficients:

$$1 - X_c(t) = \exp(-Z_t t^n) \quad (6)$$

where $X_c(t)$ is the relative crystallinity degree at time $t$, $n$ expresses the nucleation and growing geometry of the resulting crystallites and $Z_t$ is a rate constant, involving both nucleation and growth rate parameters. By expressing (6) as:

$$\log[-\ln(1 - X_c(t))] = n \log t + \log Z_t \quad (7)$$

a log[-ln(1-$X_c(t)$)] versus log$t$ plot can be used to calculate $n$ as the slope of the linear portion of the curve, and log $Z_t$ as the intercept of the same.

Under non-isothermal conditions, the Avrami approach still appropriately describes the initial stage of crystallization [7,14], therefore, in the present study, the linear fits of the Avrami plots were conducted for relative crystallinity $X_c$ between 0.03 and 0.30 (Figure 6).

$Z_t$ has been further corrected taking into account the changes in non-isothermal crystal growth due to the different cooling rate $a$ [7]:

$$\log Z_c = \frac{\log Z_t}{a} \quad (8)$$

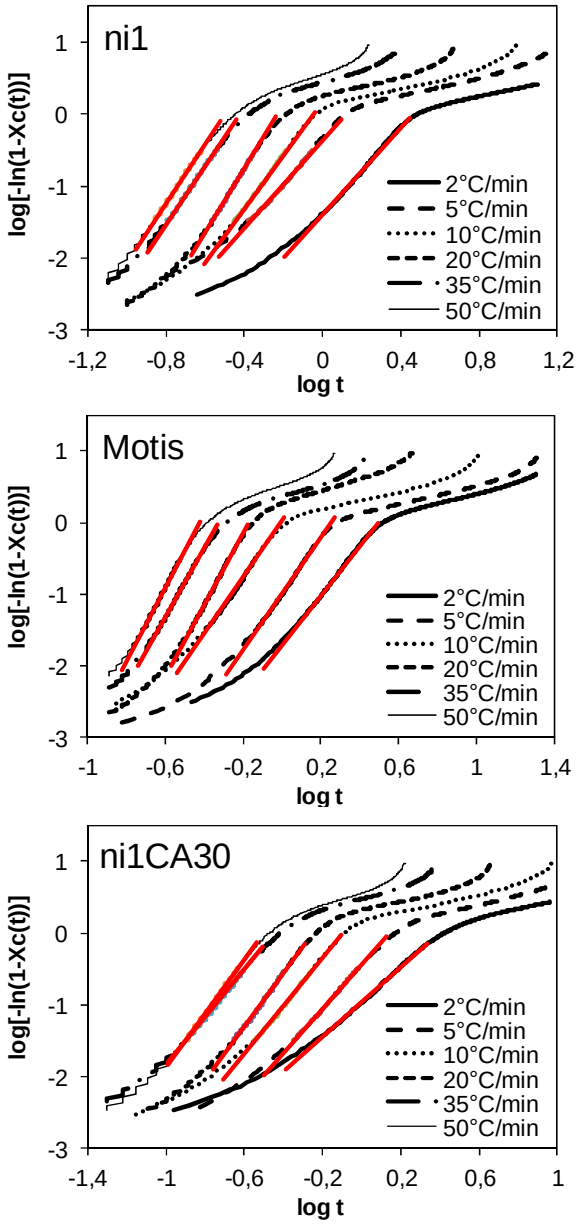


Figure 6. NI1, Motis and NI1CA30 log[-ln(1-Xc(t))] versus log t plots. The Avrami parameters were extracted from the slope and intercept of the linear portion of the curves, as indicated by the red line: log[-ln(1-Xc(t))] values in the range -1,5 – -0,5, corresponding approximately to a 3 – 30% crystallinity range.

| **Cooling rate** | **NI1** | | **Motis** | | **NI1CA30** | |
|---|---|---|---|---|---|---|
| **[°C/min]** | **n** | **Zc** | **n** | **Zc** | **n** | **Zc** |
| 2 | 3,03 | 0,19 | 3,44 | 0,14 | 2,41 | 0,33 |
| 5 | 3,23 | 0,85 | 3,94 | 0,63 | 3,08 | 0,82 |
| 10 | 3,72 | 1,04 | 3,94 | 1,00 | 3,36 | 1,08 |
| 20 | 4,43 | 1,12 | 5,05 | 1,10 | 3,70 | 1,11 |
| 35 | 4,02 | 1,11 | 4,88 | 1,11 | 3,30 | 1,10 |
| 50 | 4,12 | 1,09 | 5,17 | 1,10 | 3,82 | 1,09 |

Table 3. Calculated n and Zc, values at different cooling rates for NI1, Motis and NI1CA30.

The data reported in Table 3 for neat PEEK show that the rate constant $Z_c$ markedly increases, indicating an increase in the crystallization rate, while increasing the cooling rate from 2 °C/min to 20°C/min, while it remains almost constant for higher cooling rates. The Avrami exponent n varies approximately between 3 and 4, again with an increasing trend as the cooling rate increases up to 20°C/min, while it seems to reach a plateau for higher cooling rates.

This finding is contrast with some literature studies [7,11], in which an inverse trend of n with the cooling rate was observed and very high values of n (up to 8) were found. High Avrami exponents are generally attributed to an increasingly complex morphology of the formed crystallites, with increasing branching and increasing growth rate [11]. Cebe et al. [14] also reported that the values of n obtained by applying the Avrami equation to a non-isothermal crystallization kinetic are generally higher than those determined from the isothermal crystallization, which they ascribe to changes in the linear growth rate during non-isothermal crystallization.

On the other hand, Phillips et al. [16] found n values within the same range of those of the present study, during non-isothermal crystallization experiments of PEEK, PET, POM and PP. The Avrami exponent also showed a similar increasing trend with increasing the cooling rate. They concluded that all the four polymers must crystallize through three dimensional spherulitic growth, with a predominant heterogeneous nucleation at low cooling rates and a predominant homogeneous nucleation at high cooling rates.

Our findings confirm this interpretation. It must be pointed out, though, that all the cited studies used different PEEK resins, whose structural characteristics (i.e. molecular weight) were mainly not reported: this can partly explain the observed differences.

CFR PEEK showed the same n and $Z_c$ trend with the cooling rate, but n values at the same cooling rate for Motis CFR PEEK were systematically higher than for NI1, unfilled PEEK, while NI1CA30 had lower n values compared to NI1. This further indicates that the two fiber reinforces demonstrate an opposite effect on the resulting morphology. In particular, Motis CFR PEEK generally seems to develop a more complex morphology than NI1 unfilled PEEK, while NI1CA30 shows the opposite trend, presumably due to the smaller space between fibers caused by the higher fiber density within the polymer.

### *3.5 Kinetic analysis by Avrami-Ozawa equation*

In order to check the accuracy of the results, the crystallization data were also elaborated with the Avrami-Ozawa approach, which is generally considered to be more consistent for non-isothermal crystallization [17,24], despite with this model is still not possible to overcome the linear time dependant crystal growth, which limits the possibility to represent the crystallization behavior as a

function of a complex thermal history [30]. To present though, there is practically no literature available on modeling such behaviors, or, if any, the proposed models have still to be adapted and validated for specific materials [30], therefore the discussion herein will be limited to the results obtained from the Avrami and Avrami-Ozawa approaches.

For a rate dependent process, the Avrami equation can be modified into the Ozawa equation by replacing *t* in equation 6, as follows

$$1 - X_c(T) = \exp - \left[\frac{K(T)}{|a|^m}\right] \tag{9}$$

or:

$$\log[-\ln(1 - X_c(T))] = \log K(T) - m \log a \tag{10}$$

where $X_c(T)$ is the relative degree of crystallization at temperature T, $K(T)$ is a cooling function depending on the overall crystallization rate, and *m* is the Ozawa exponent, depending on the crystal growth and nucleation mechanism. The Ozawa equation was already proven not adequate to appropriately describe the non-isothermal crystallization kinetics of some polymer systems, including PEEK [14]. However, by combining equation (5) with (2), Liu at al [17] elaborated a combined Avrami-Ozawa equation, as follows:

$$n \log t + \log Z_t = \log K(T) - m \log a \tag{11}$$

which can be expressed as:

$$\log a = \log F(T) - b \log t \tag{12}$$

where the parameters $F(T)$ and $b$ are equal to $[K(T)/Z_t]^{1/m}$ and $n/m$, respectively. The equation relates the cooling rate *a* to the crystallization time *t*, under dynamic crystallization condition, for a given degree of crystallization. According to equation 12, at a given degree of crystallization, a plot of log *a* against log *t* will give a straight line, and $-b$ and $F(T)$ will be derived from the slope and the intercept of the plots, respectively (Figure 7).

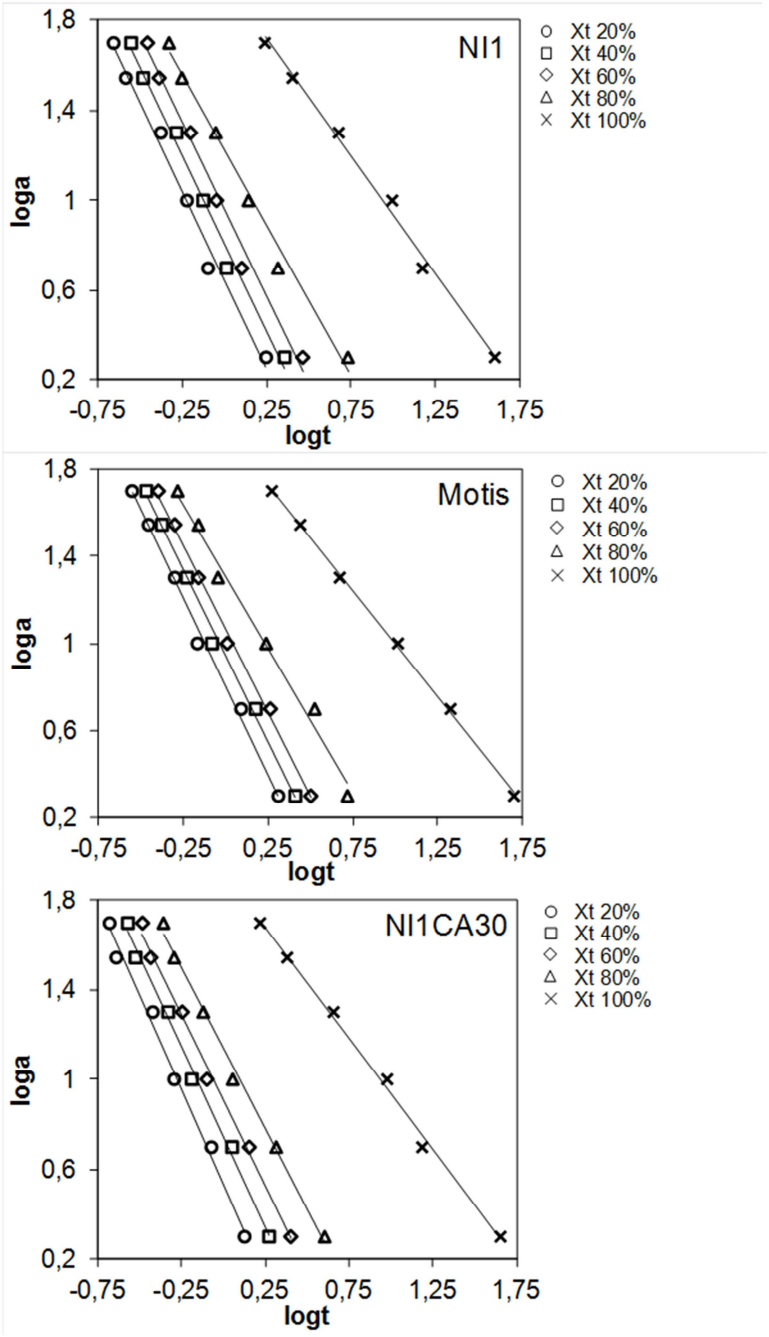

Figure 7. NI1, Motis and NI1CA30 loga versus logt plots.

The Avrami-Ozawa parameters for each material and relative crystallinity are summarized in Table 4. For each crystallization stage considered, data fit on a straight line, indicating that the model is suitable for describing the crystallization kinetics of all three PEEK formulations [19,31]. The b coefficient remains reasonably constant for the initial stages of crystallization (relative crystallinity lower than 60%), while it decreases at higher relative crystallinities, independently on the presence of the CF reinforce, confirming the presence of a slow secondary crystallization regime for high degree of relative crystallinity. Hsiao et al. [12] and Fougnies et al [6], based on SAXS, WAXS, and DSC crystallization studies hypothesized that the primary process, occurring in the unrestrained

melt, produces thicker lamellar stacks, while the secondary crystallization, occurring in the restrained melt during the spherulite-impingement stage, results in a small fraction of thinner lamellae.

The theoretical meaning of F(T) refers to the value of cooling rate, which has to be chosen at unit crystallization time when the measured system amounts to a certain degree of crystallinity [17]. As expected, F(T) showed a steady increase with the relative crystallinity, indicating that, at unit crystallization time, a higher cooling rate should be used in order to obtain a higher degree of crystallinity [19,24]. By comparing the F(T) values among the three different PEEK formulations, it can be noted that NI1CA30 showed lower values if compared to unfilled PEEK, while Motis had higher F(T) coefficient for each degree of crystallization considered. (Table 4).

| X(T) | NI1 | | Motis | | NI1CA30 | |
|---|---|---|---|---|---|---|
| [%] | b | logF(T) | b | logF(T) | b | logF(T) |
| 20 | 1.57 | 0.65 | 1.61 | 0.80 | 1.67 | 0.54 |
| 40 | 1.56 | 0.81 | 1.57 | 0.94 | 1.60 | 0.75 |
| 60 | 1.54 | 0.96 | 1.54 | 1.07 | 1.53 | 0.91 |
| 80 | 1.33 | 1.22 | 1.32 | 1.31 | 1.42 | 1.14 |
| 100 | 1.04 | 1.97 | 0.97 | 1.97 | 0.99 | 1.93 |

Table 4. Calculated -*b* and *F*(*T*) values at different cooling rates or *X*(*T*) values for NI1, Motis and NI1CA30.

*3.6 Crystallinity of non-isothermally crystallized samples*

In order to verify the indications of the above illustrated approaches, post crystallization DSC analyses have been performed to evaluate the samples resulting crystallinity.

The DSC thermograms resulting from this experiment evidenced a typical double-melting behavior, which is much more evident for the samples crystallized at low cooling rates (Figure 8), while it is almost negligible for higher values of cooling rates. The crystallization enthalpies, glass transition ($T_g$) and melting peak ($T_{m1}$, $T_{m2}$) temperatures are listed in Table 5.

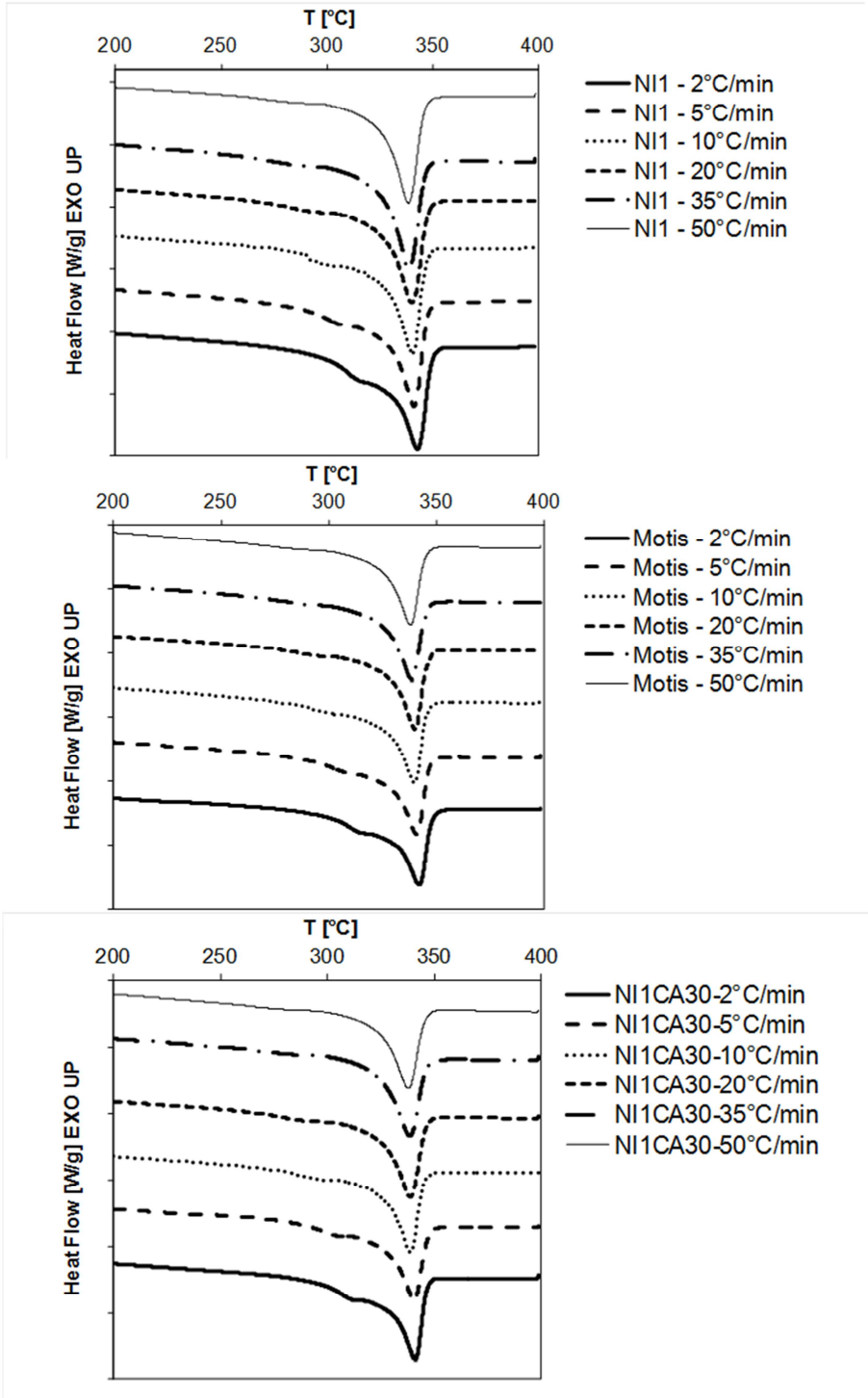


Figure 8. Heating curves of NI1, Motis, and NI1CA30 after the non-isothermal crystallization study. All melting experiments were run at a constant heating rate of 20°C/min. The rate in the figure indicates the cooling rate used during the previous crystallization experiments.

| Material | Cooling rate [°C/min] | Corrected $\Delta H_m$ [J/g] | X [%] | $T_g$ [°C] | $T_{m1}$ [°C] | $T_{m2}$ [°C] |
|---|---|---|---|---|---|---|
| NI1 PEEK (unfilled) | 2 | 51.8 ± 0.9 | 39.9 | 145 | 314 | 343 |
| | 5 | 48.7 ± 0.7 | 37.5 | 144 | 306 | 341 |

| | | | | | | |
|---|---|---|---|---|---|---|
| | 10 | 47.9 ± 0.3 | 36.9 | 145 | 297 | 340 |
| | 20 | 45.1 ± 0.4 | 34.7 | 144 | 291 | 340 |
| | 35 | 45.5 ± 0.4 | 34.9 | 145 | 285 | 339 |
| | 50 | 41.7 ± 0.2 | 32.1 | 146 | 281 | 338 |
| NI1CA30 PEEK (30% wt PAN CFR) | 2 | 49.7 ± 0.8 | 38.2 | 140 | 311 | 341 |
| | 5 | 46.6 ± 0.5 | 35.8 | 141 | 303 | 340 |
| | 10 | 45.5 ± 0.4 | 35.0 | 141 | 296 | 339 |
| | 20 | 43.8 ± 0.3 | 33.7 | 142 | 288 | 339 |
| | 35 | 42.8 ± 0.2 | 32.9 | 141 | 279 | 339 |
| | 50 | 40.7 ± 0.1 | 31.3 | 142 | 275 | 338 |
| Motis PEEK (30% wt pitch CFR) | 2 | 55.6 ± 0.2 | 42.8 | 141 | 314 | 342 |
| | 5 | 51.3 ± 0.2 | 39.5 | 142 | 308 | 341 |
| | 10 | 50.2 ± 0.8 | 38.6 | 141 | 300 | 340 |
| | 20 | 45.8 ± 0.5 | 35.2 | 144 | 294 | 340 |
| | 35 | 46.7 ± 0.5 | 35.9 | 144 | 288 | 339 |
| | 50 | 42.6 ± 0.2 | 32.8 | 143 | 280 | 338 |

Table 5. Glass transition and peak melting temperatures, crystallization enthalpies and calculated crystallinity for NI1, Motis, and NI1CA30 at different cooling rates.

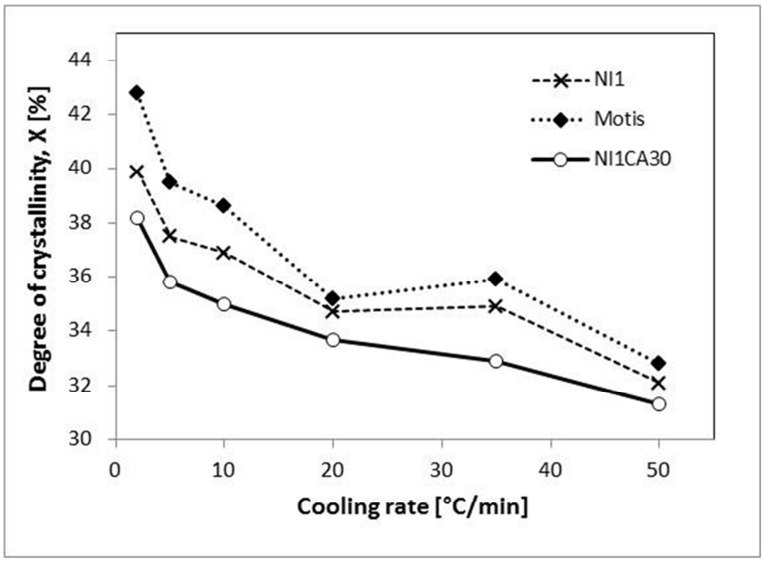


Figure 9. Cristallinity measured as a function of the cooling rate.

The overall % crystallinity decreases as the cooling rate increases for all PEEK formulations. At each cooling rate, the crystallinity is higher for Motis CFR PEEK and lower for NI1CA30, when compared to neat PEEK (NI1). This is in accordance to what observed in the previous analyses.

The glass transition temperature ($T_g$) does not show a definite trend as the cooling rate increases and the crystallinity decreases. It has been reported that, although depending on the detailed structure of the polymer, the non-crystal region may also be affected by different crystallization degrees, in that the mobility of the molecules adjacent to crystals may be assumed to be restricted [32,33]. It might be also hypothesized that the presence of the carbon fibers equally acts as a constraint to the mobility of the amorphous fraction, resulting in a Tg increase. Both these assumptions clearly do not apply to the present case. On the contrary, the $T_g$ of the unfilled polymer was constantly a few degrees higher than that of the two CFR PEEKs. Similar findings were previously interpreted by various authors [30,34,35] in terms of a two layer model. According to this model, an interfacial layer with constrained chain mobility is developed near to the filler, due to interaction with the fibers surface. On the other hand, the presence of the filler in the polymer bulk, may induce a decrease of density and, consequently, an increase of free volume, as experimentally observed in several polymer composites. As a result, the molecular mobility of the polymer chains in the matrix bulk increases, allowing the cooperative motion of the chains at lower temperature, which in turn results in the observed reduction of the glass transition temperature. It was also speculated that the existence of two different amorphous regions should not mean necessarily the appearance of two glass transitions in the DSC thermograms, as this technique may be not sensitive enough to reveal such small changes [34,35].

The lower melting temperature ($T_{m1}$) varies with the cooling rate and systematically occurs few degrees above the corresponding crystallization temperature ($T_{c,}$ see Table 1) for all PEEK formulations. On the contrary, the higher melting temperature ($T_{m2}$) shows only a slight decrease as the cooling rate increases.

Two opposite interpretation of PEEK's double melting peak can be found in the literature: some researchers suggested that the two endotherms represent the melting of two morphologically different crystal populations grown during crystallization [5,36], while most of the recent studies attributed the multiple endotherms to a combination of a melting – recrystallization – remelting process of the original crystals [8,9]. On support of the latter hypothesis, Tardif and co-workers [9] demonstrated that, when heating an isothermally crystallized sample fast enough (5000K/s) to suppress recrystallization, only a single melting peak is observed. Lee and Porter [8] postulated that the low-temperature endotherm represents only a portion of the melting endotherm of the original crystals: a reorganization process is believed to occur at crystal surfaces through a partial melting followed by recrystallization. The high temperature endotherm is the melting of crystals reorganized during the heating scan.

Crystal surfaces are metastable due to the existence of chain folds, loops, cilia, and tie molecules; Krüger and Zachmann [33] have also suggested that melting and recrystallization can occur at the crystal surface, even when the overall crystal is stable.

These observations support the hypothesis that the observed thermal behavior is the result of a reorganization during the heating scan. This reorganization process, occurring at the crystal surfaces, may also prevent some core crystalline portions from melting [8].

In our case, given the constant heating rate, the samples non-isothermally crystallized at lower cooling rates showed higher $T_{m1}$, because bigger crystals (thicker lamellae) have formed during crystallization on cooling. A larger extent of reorganization in the samples crystallized at lower cooling rates accounts for an overall higher crystallinity and for the formation of bigger crystals, which finally melt at higher temperature ($T_{m2}$). On the contrary, those crystallized at high cooling rates showed smaller endotherm at lower $T_{m1}$, due to a lower amount of second order crystals formed during the crystallization step. The overall cristallinity percentage should be therefore decreasing as the cooling rate increases for all PEEK formulations, as experimentally observed.

## 4. Conclusions

The results of this study show that melt crystallization of PEEK and CFR-PEEK is governed by complex mechanisms. The addition of the same weight percentage of a reinforcement fiber can influence the polymer crystallization by either favoring or hindering the crystallization, depending on the fibers characteristics and geometry, which trigger a competition between heterogeneous nucleation on fiber surfaces and reduced crystallization in the restricted spaces between fibers. Crystallization kinetics, activation energies and resulting crystallinity investigated in the present study have shown to vary according to those principles.

Further, changing the cooling rate from the molten state during crystallization influences the crystal growth process, resulting in a decrease of the extent of secondary crystallization for higher cooling rates.

Overall, these results suggest that processing conditions and fiber reinforcement have to be accurately selected in order to ensure an optimal polymer morphology. In fact, it has been demonstrated that different morphologies might result from different cooling regimes, even though further studies are needed to better characterize the extent of this phenomenon, especially in light of the simultaneous melting and re-organization of crystals that occurs during the sample heating.

In order to gain a better insight into this phenomenon, our future studies will aim to investigate the polymer crystallinity after the melt crystallization by differentiating the heating rate, as well as to assess the crystal morphology by microscopy techniques.

**References**


[1] S.M. Kurtz, J.N. Devine, PEEK biomaterials in trauma, orthopedic, and spinal implants, Biomaterials. 28 (2007) 4845–4869. doi:10.1016/j.biomaterials.2007.07.013.

[2] M. Biron, Thermoplastics and thermoplastic composites 2nd ed., Plast. Des. Libr. (2013).

[3] Y. Lee, R.S. Porter, Crystallization of poly(etheretherketone) (PEEK) in carbon fiber composites, Polym. Eng. Sci. 26 (1986) 633–639.

[4] D.J. Blundell, B.N. Osborn, The morphology of poly(aryl-ether-ether-ketone), Polymer (Guildf). 24 (1983) 953–958. doi:10.1016/0032-3861(83)90144-1.

[5] S.C. Chao, M. Chen, C.T. Chung, Isothermal crystallization and melting behavior of short carbon fiber reinforced poly(ether ether ketone) composites, J. Polym. Res. 5 (1998) 221–226.

[6] C. Fougnies, P. Damman, M. Dosière, M.H.J. Koch, Time-resolved SAXS, WAXS, and DSC study of melting of poly(aryl ether ether ketone) (PEEK) annealed from the amorphous state, Macromolecules. 30 (1997) 1392–1399.

[7] M.C. Kuo, J.C. Huang, M. Chen, Non-isothermal crystallization kinetic behavior of alumina nanoparticle filled poly(ether ether ketone), Mater. Chem. Phys. 99 (2006) 258–268. doi:10.1016/j.matchemphys.2005.10.021.

[8] Y. Lee, R.S. Porter, Double-melting behavior of poly (ether ether ketone), Macromolecules. 20 (1987) 1336–1341. doi:10.1021/ma00172a028.

[9] X. Tardif, B. Pignon, N. Boyard, J.W.P. Schmelzer, V. Sobotka, D. Delaunay, et al., Experimental study of crystallization of PolyEtherEtherKetone (PEEK) over a large temperature range using a nano-calorimeter, Polym. Test. 36 (2014) 10–19. doi:10.1016/j.polymertesting.2014.03.013.

[10] L. Jin, J. Ball, T. Bremner, H.J. Sue, Crystallization behavior and morphological characterization of poly(ether ether ketone), Polym. (United Kingdom). 55 (2014) 5255–5265. doi:10.1016/j.polymer.2014.08.045.

[11] Y. Seo, S. Kim, Nonisothermal Crystallization Behavior of Poly(ary1 ether ether ketone), Polym. Eng. Sci. 41 (2001) 940–945. doi:10.1002/pen.10793.

[12] B.S. Hsiao, K.H. Gardner, D.Q. Wu, B. Chu, Time-resolved X-ray study of poly(aryl ether ether ketone) crystallization and melting behaviour: 1. Crystallization, Polymer (Guildf). 34 (1993) 3986–3995. doi:10.1016/0032-3861(93)90658-W.

[13] C.L. Wei, M. Chen, F.E. Yu, Temperature modulated DSC and DSC studies on the origin of double melting peaks in poly(ether ether ketone), Polymer (Guildf). 44 (2003) 8185–8193. doi:10.1016/j.polymer.2003.10.009.

[14] P. Cebe, S.D. Hong, Crystallization behaviour of poly(ether-ether-ketone), Polymer (Guildf). 27 (1986) 1183–1192. doi:10.1016/0032-3861(86)90006-6.

[15] M. Chen, C.T. Chung, Crystallinity of isothermally and nonisothermally crystallized poly(ether ether ketone) composites, Polym. Compos. 19 (1998) 689–697.

[16] R. Phillips, J.E. Ma, Prediction and Analysis of Nonisothermal Crystallization of Polymers, J. Polym. Sci. Part B Polym. Phys. 35 (1997) 875–888.

[17] T. Liu, Z. Mo, S. Wang, H. Zhang, Nonisothermal melt and cold crystallization kinetics of poly(Aryl Ether Ether Ketone Ketone), Polym. Eng. Sci. 37 (1997) 568–575.

[18] M.C. Kuo, J.S. Kuo, M.H. Yang, J.C. Huang, On the crystallization behavior of the nano-silica filled PEEK composites, Mater. Chem. Phys. 123 (2010) 471–480. doi:10.1016/j.matchemphys.2010.04.043.

[19] M. Sattari, A. Molazemhosseini, M.R. Naimi-Jamal, A. Khavandi, Nonisothermal crystallization behavior and mechanical properties of PEEK/SCF/nano-SiO2 composites, Mater. Chem. Phys. 147 (2014) 942–953. doi:10.1016/j.matchemphys.2014.06.041.

[20] M. Regis, S. Fusi, R. Favaloro, P. Bracco, Composite Science and Technology 2020 - Scientific and Technical Challenges, in: 9th Int. Conf. Compos. Sci. Technol., DEStech Publications Inc (USA), Sorrento, Italy, 2013: pp. 44–56.

[21] E. Bessard, O. De Almeida, G. Bernhart, Unified isothermal and non-isothermal modelling of neat PEEK crystallization, J. Therm. Anal. Calorim. 115 (2014) 1669–1678. doi:10.1007/s10973-013-3308-8.

[22] T.F.J. Pijpers, V.B.F. Mathot, B. Goderis, R.L. Scherrenberg, E.W. van der Vegte, High-Speed Calorimetry for the Study of the Kinetics of (De)vitrification, Crystallization, and Melting of Macromolecules, Macromolecules. 35 (2002) 3601–3613. doi:10.1021/ma011122u.

[23] E. Zhuravlev, J.W.P. Schmelzer, B. Wunderlich, C. Schick, Kinetics of nucleation and crystallization in poly(ε-caprolactone) (PCL), Polymer (Guildf). 52 (2011) 1983–1997. doi:10.1016/j.polymer.2011.03.013.

[24] T. Liu, Z. Mo, H. Zhang, Nonisothermal crystallization behavior of a novel poly(aryl ether ketone): PEDEKmK, J. Appl. Polym. Sci. 67 (1998) 815–821.

[25] S. Vyazovkin, Is the Kissinger equation applicable to the processes that occur on cooling?, Macromol. Rapid Commun. 23 (2002) 771–775.

[26] M. Run, H. Song, C. Yao, Y. Wang, Crystal morphology and nonisothermal crystallization kinetics of short carbon fiber/poly(trimethylene terephthalate) composites, J. Appl. Polym. Sci. 106 (2007) 868–877. doi:10.1002/app.26661.

[27] M. Avrami, Kinetics of phase change. I: General theory, J. Chem. Phys. 7 (1939) 1103–1112.

[28] M. Avrami, Kinetics of phase change. II Transformation-time relations for random distribution of nuclei, J. Chem. Phys. 8 (1940) 212–224.

[29] M. Avrami, Granulation, phase change, and microstructure kinetics of phase change. III, J. Chem. Phys. 9 (1941) 177–184.

[30] A. Lion, M. Johlitz, A thermodynamic approach to model the caloric properties of semicrystalline polymers, Contin. Mech. Thermodyn. 28 (2015) 799–819. doi:10.1007/s00161-015-0415-8.

[31] S.H. Kim, S.H. Ahn, T. Hirai, Crystallization kinetics and nucleation activity of silica nanoparticle-filled poly(ethylene 2,6-naphthalate), Polymer (Guildf). 44 (2003) 5625–5634. doi:10.1016/S0032-3861(03)00623-2.

[32] G.M.K. Ostberg, J.C. Seferis, Annealing effects on the crystallinity of polyetheretherketone (PEEK) and its carbon fiber composite, J. Appl. Polym. Sci. 33 (1987) 29–39.

[33] K.N. Krüger, H.G. Zachmann, Investigation of the melting behavior of poly(aryl ether ketones) by simultaneous measurements of SAXS and WAXS employing synchrotron radiation, Macromolecules. 26 (1993) 5202–5208.

[34] D. Fragiadakis, P. Pissis, L. Bokobza, Glass transition and molecular dynamics in poly(dimethylsiloxane)/silica nanocomposites, Polymer (Guildf). 46 (2005) 6001–6008. doi:10.1016/j.polymer.2005.05.080.

[35] E. Logakis, C. Pandis, V. Peoglos, P. Pissis, C. Stergiou, J. Pionteck, et al., Structure-property relationships in polyamide 6/multi-walled carbon nanotubes nanocomposites, J. Polym. Sci. Part B Polym. Phys. 47 (2009) 764–774. doi:10.1002/polb.21681.

[36] D.C. Bassett, R.H. Olley, I.A.M. Al Raheil, On crystallization phenomena in PEEK, Polymer (Guildf). 29 (1988) 1745–1754. doi:10.1016/0032-3861(88)90386-2.